Hindawi
Mathematical Problems in Engineering
Volume 2023, Article ID 2715787, 18 pages
https://doi.org/10.1155/2023/2715787

Research Article

Effect of Suspension Roll Angle Sensors on the Performance of H_∞ Active Antiroll Bar Control System of Trucks

Van Tan Vu [1] **and Ngoc Tuan Vu** [2]

[1]*Department of Automotive Mechanical Engineering, Faculty of Mechanical Engineering, University of Transport and Communications, Hanoi, Vietnam*
[2]*Department of Automotive Engineering, Faculty of Vehicle and Energy Engineering, Le Quy Don Technical University, Hanoi, Vietnam*

Correspondence should be addressed to Ngoc Tuan Vu; tuan.vungoc@lqdtu.edu.vn

Received 6 October 2022; Revised 12 December 2022; Accepted 21 December 2022; Published 17 January 2023

Academic Editor: Laurent Dewasme

The rollover phenomenon is quite familiar with trucks and often has severe consequences worldwide. This article focuses on developing a new control structure for the active antiroll bar system using the robust control method. The main objective is to improve the vehicle's roll stability by using additional suspension roll angle sensors. First, a truck model equipped with an active antiroll bar system is introduced. Then, the basic robust controller structure diagram is described in detail. Based on this basic robust controller, the authors develop a new robust controller considering the suspension roll angle sensors. Finally, the response of a truck using an active antiroll bar system with two robust (H_∞) controllers and a passive antiroll bar system is compared and evaluated in the time domain and in the frequency domain. The results showed that the use of two sensors of the suspension roll angle sensors increased the efficiency by about 20% compared to the basic robust controller. This has proven the effectiveness of a new approach in improving the roll stability of trucks.

1. Introduction

The rollover of automobiles and trucks is a serious traffic safety problem worldwide. Although rollover accidents happen infrequently, they cause serious consequences for human life, the economy, and traffic infrastructure [1, 2]. In order to improve the roll stability of trucks, modern control solutions have been studied and applied, such as active braking system [3], active antiroll bar system [4–6], active steering system [7–9], and active suspension [10]. Among these systems, the active antiroll bar system directly meets the goal of preventing rollover and is gradually being perfected to be fitted to commercial vehicles soon.

The active antiroll bar system for trucks is composed of two electro-hydraulic actuators on either side of the dependent suspension system as shown in Figure 1. For each actuator, one end is linked to the vehicle body, and the other end is linked to the unsprung mass. When the actuators create forces equal in magnitude and opposite in direction, the system generates an active torque against the vehicle's overturning. Antiroll torque control is achieved through the oil flow pressure regulation via a solenoid valve [12–14]. The main research directions related to the active antiroll bar system on trucks can be mentioned as follows:

(i) *Building Vehicle Model.* The models used include the roll model [11], the yaw-roll model [4–6], and the actuator model [14]. These models establish the stabilizing moment of the active antiroll bar system acting on the part of the sprung mass and unsprung mass in the roll plane. The main control signal is the torque of the active antiroll bar system or the input current supplied to the system when combined with the actuator model.

(ii) *Designing Controller.* Some of the control methods applied to the active antiroll bar control system on

trucks are briefly recalled in the following: (1) Optimal control: Sampson and Cebon [13, 15, 16] proposed a state feedback controller which was designed by finding an optimal controller based on a linear quadratic regulator (LQR) for single-unit and heavy articulated vehicles. The LQR was also applied to an integrated model, including an electronic servo-valve hydraulic actuator model and a yaw-roll model of a single-unit heavy vehicle. The input current of the electronic servo-valve is the input control signal [17, 18]. (2) Neural network control: a reinforcement learning algorithm using neural networks is proposed to improve the roll stability for a single-unit heavy vehicle [1, 10, 19].

(iii) Robust control (LPV): Gaspar et al. [2, 4–6] applied linear parameter-varying techniques to control active antiroll bars combined with active brakes on the single-unit heavy vehicle. The forward velocity is considered the varying parameter.

The robust control method is applied to the active antiroll bar system on trucks to improve the vehicle's roll stability. The sensors used are mainly the lateral acceleration sensor and the velocity of the sprung mass roll angle. When the truck approaches the lateral instability state, the lateral acceleration value rapidly increases. Furthermore, the lateral acceleration sensor is inexpensive and highly accurate [20]. Therefore, the lateral acceleration sensor is most often used to control the active antiroll bar system. The velocity of the sprung mass roll angle sensor is also used a lot for the above purpose. However, no studies have used the suspension roll angle sensor to control the active antiroll bar system. Meanwhile, the control goal is to maintain the magnitude of this angle not exceeding 7-8 degrees [2, 4, 21, 22].

Based on the previous research using the genetic algorithm method to find the optimal weighting function of the robust controller for the active antiroll bar system in the 15th Mini Conference on Vehicle System Dynamics, Identification, Anomalies, Budapest, and Hungary [23], the main contributions of this paper can be listed as follows:

(i) Building a basic H_∞ control structure for the active antiroll bar system (first H_∞ active antiroll bar controller) using two common sensors: the lateral acceleration sensor and the sprung mass roll angle velocity sensor. This control structure is built on a truck model with an active antiroll bar system equipped at the two axles.

Figure 1: Active antiroll bar system on real trucks [11].

(ii) A new H_∞ control structure (second H_∞ active antiroll bar controller) is built using two suspension roll angle sensors. At the same time, these two signals' magnitude values are considered the performance output that should be minimized.

The structure of the paper is organized as follows: Section 2 introduces the truck model, with the control signal being the torque of the active antiroll bar system. Section 3 introduces H_∞ controller design with a basic structure and proposes a new structure. Evaluating the effectiveness of the proposed controller in the frequency domain is shown in Section 4, and the time domain is detailed in Section 5. The conclusions and further research directions are presented in Section 6.

2. Truck Modeling to Study Roll Stability

2.1. Yaw-Roll Model of a Truck. Figure 2 illustrates the combined yaw-roll dynamics of a truck modeled by a three-body system, where m_s is the sprung mass, m_{uf} the unsprung mass at the front, including the front wheels and axle, and m_{ur} the unsprung mass at the rear, with the rear wheels and axle. The model variables are given in Table 1 and the parameters are in [2].

In the vehicle modeling, the differential equations of motion of the yaw-roll dynamics of the truck, i.e., the lateral dynamics (1), the yaw moment (2), the roll moment of the sprung mass (3), the roll moment of the front (4), and the rear and unsprung masses (5). They are formalized in the equations (6).

$$\left\{ mv(\dot{\beta} + \dot{\psi}) - m_s h\ddot{\phi} = F_{yf} + F_{yr}, \right. \tag{1}$$

$$\left\{ -I_{xz}\ddot{\phi} + I_{zz}\ddot{\psi} = F_{yf} l_f - F_{yr} l_r, \right. \tag{2}$$

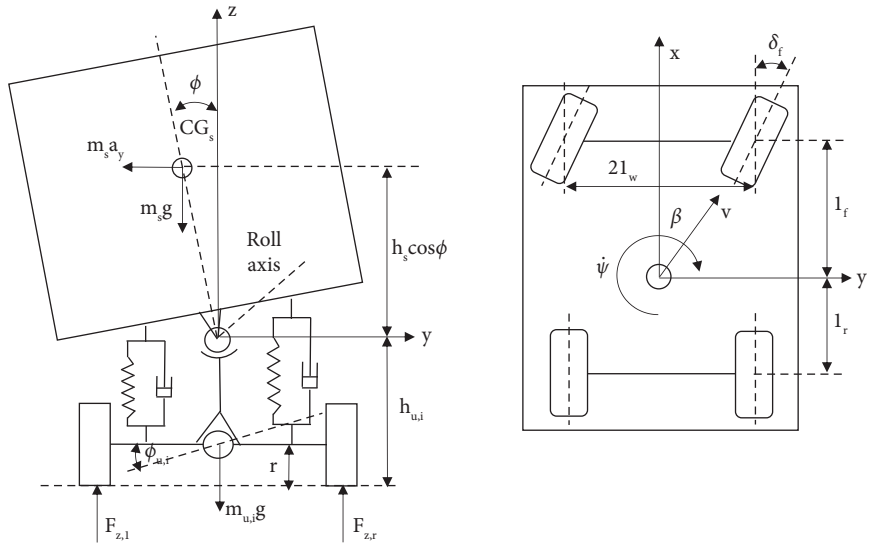

Figure 2: Yaw-roll model of a truck [2, 4].

Table 1: Variables of the yaw-roll model [2, 4].

Symbols	Description	Values
m_s	Sprung mass	12487 kg
$m_{u;f}$	Unsprung mass on the front axle	706 kg
$m_{u;r}$	Unsprung mass on the rear axle	1000 kg
m	The total vehicle mass	14193 kg
h	Height of CG of sprung mass from the roll axis	1.15 m
$h_{u;i}$	Height of CG of unsprung mass from the ground	0.53 m
r	Height of roll axis from the ground	0.83 m
C_f	Tire cornering stiffness on the front axle	582×10^3 kN/rad
C_r	Tire cornering stiffness on the rear axle	783×10^3 kN/rad
k_f	Suspension roll stiffness on the front axle	380×103 kNm/rad
k_r	Suspension roll stiffness on the rear axle	684×10^3 kNm/rad
b_f	Suspension roll damping on the front axle	100×10^3 kN/rad
b_r	Suspension roll damping on the rear axle	100×10^3 kN/rad
k_{tf}	Tire roll stiffness on the front axle	2060×10^3 kNm/rad
k_{tr}	Tire roll stiffness on the rear axle	3337×10^3 kNm/rad
I_{xx}	Roll moment of inertia of sprung mass	24201 kgm^2
I_{xz}	Yaw-roll product of inertia of sprung mass	4200 kgm^2
I_{zz}	Yaw moment of inertia of sprung mass	34917 kgm^2
l_f	Length of the front axle from the CG	1.95 m
l_r	Length of the rear axle from the CG	1.54 m
l_w	Half of the vehicle width	0.93 m
μ	Road adhesion coefficient	1
v	Forward velocity	—
v_{wi}	Components of the forward velocity	—
a_y	Lateral acceleration	—
β	Side-slip angle at the center of mass	—
$\dot{\psi}$	Heading angle	—
ψ	Yaw rate	—
α	Side slip angle	—
ϕ	Sprung mass roll angle	—
$\phi_{u,i}$	Unsprung mass roll angle	—
δ_f	Steering angle	—

$$\begin{cases} \left(I_{xx} + m_s h^2\right)\ddot{\phi} - I_{xz}\ddot{\psi} = m_s g h \phi + m_s v h (\dot{\beta} + \dot{\psi}) - k_f\left(\phi - \phi_{uf}\right) - b_f\left(\dot{\phi} - \cdot \phi_{uf}\right) + M_{ARf} + U_f \\ -k_r\left(\phi - \phi_{ur}\right) - b_r\left(\dot{\phi} - \cdot \phi_{ur}\right) + M_{ARr} + U_r, \end{cases} \tag{3}$$

$$\left\{-rF_{yf} = m_{uf} v\left(r - h_{uf}\right)(\dot{\beta} + \dot{\psi}) + m_{uf} g h_{uf} \phi_{uf} - k_{tf}\phi_{uf} + k_f\left(\phi - \phi_{uf}\right) + b_f\left(\dot{\phi} - \cdot \phi_{uf}\right) + M_{ARf} + U_f, \right. \tag{4}$$

$$\left\{-rF_{yr} = m_{ur} v\left(r - h_{ur}\right)(\dot{\beta} + \dot{\psi}) - m_{ur} g h_{ur} \phi_{ur} - k_{tr}\phi_{ur} + k_r\left(\phi - \phi_{ur}\right) + b_r\left(\dot{\phi} - \cdot \phi_{ur}\right) + M_{ARr} + U_r, \right. \tag{5}$$

where U_f, U_r are the torques at the two axles; F_{yf}, F_{yr} the lateral tyre forces; M_{ARf}, M_{ARr} the moments of the passive antiroll bar, which impact the unsprung and sprung masses at the front and rear axles [14].

By using the previous equation, the truck can be represented by the linear system in the state space representation (6):

$$\begin{cases} \dot{x} = Ax + B_1 w + B_2 u, \\ y = Cx, \end{cases} \tag{6}$$

with the state vector: $x = [\beta \dot{\psi} \phi \dot{\phi} \varphi_{uf} \varphi_{ur}]^T$, the disturbance input: $w = [\delta_f]$, the control inputs: $u = [U_f U_r]^T$, and the output vector: $y = [\beta \dot{\psi} \phi \dot{\phi} \varphi_{uf} \varphi_{ur}]^T$. The matrices A, B_1, and B_2 are defined as in Appendix.

2.2. Actuator of the Active Antiroll Bar System. Figure 3 illustrates the diagram of a hydraulic cylinder in combination with an electronic servo-valve. The symbols of the actuator are shown in Table 2. The spool valve of the electronic servo-valve is controlled by a current, which generates a displacement x_v. The high-pressure oil supply P_s is always stored outside the electronic servo valve, and the moving spool valve distributes the high-pressure oil into two chambers of the hydraulic cylinder. The difference of pressure $\Delta P = P_1 - P_2$ between the two chambers produces the output force F_{act} given by

$$F_{\text{act}} = A_P \Delta P, \tag{7}$$

where A_P is the area of the piston, the equations for each chamber of the hydraulic cylinder can be written as

$$\begin{cases} \dfrac{dV_1}{dt} + \dfrac{V_1}{\beta_e}\dfrac{dP_1}{dt} = Q_1 - C_{ip}(P_1 - P_2) - C_{ep}P_1, \\ \dfrac{dV_2}{dt} + \dfrac{V_2}{\beta_e}\dfrac{dP_2}{dt} = C_{ip}(P_1 - P_2) - C_{ep}P_2 - Q_2, \end{cases} \tag{8}$$

where β_e is the effective bulk modulus of the oil, C_{ep} and C_{ip} are the hydraulic cylinder's external and internal leakage coefficients.

The volume in each chamber varies with the piston displacement y_a, as

$$\begin{cases} V_1 = V_{01} + A_p y_a, \\ V_2 = V_{02} - A_p y_a, \end{cases} \tag{9}$$

where V_{01} and V_{02} are the initial volumes in each chamber. In assuming that $V_{01} = V_{02} = V_0$, the total volume of trapped oil is given by (10)

$$V_t = V_1 + V_2 = V_{01} + V_{02} = 2V_0. \tag{10}$$

Therefore, the equations in each chamber become

$$\begin{cases} A_P\dfrac{dy_a}{dt} + \dfrac{V_0 + A_P y_a}{\beta_e}\dfrac{dP_1}{dt} = Q_1 - C_{ip}(P_1 - P_2) - C_{ep}P_1, \\ -A_P\dfrac{dy_a}{dt} + \dfrac{V_0 - A_P y_a}{\beta_e}\dfrac{dP_2}{dt} = C_{ip}(P_1 - P_2) - C_{ep}P_2 - Q_2. \end{cases} \tag{11}$$

Subtracting the second equation from the first one leads to

$$2Q_L = Q_1 + Q_2 = 2C_{tp}\Delta P + 2A_p\frac{dy_a}{dt} + \frac{V_0}{\beta_e}\frac{d\Delta P}{dt}, \tag{12}$$

where $C_{tp} = 2C_{ip} + C_{ep}$ is the total leakage coefficient of the hydraulic cylinder.

From equations (8) to (12), the dynamic equation of the servo-valve hydraulic cylinder is obtained as follows:

$$\frac{V_t}{4\beta_e}\frac{d\Delta P}{dt} + \left(K_P + C_{tp}\right)\Delta P - K_x X_v + A_P\frac{dy_a}{dt} = 0, \tag{13}$$

where y_a is the displacement of the piston inside the hydraulic cylinder.

The three-land-four-way spool valve is used in the actuator. The displacement of the spool valve x_v is controlled by the electrical current u. The effects of hysteresis and flow forces on the servo-valve are neglected here, and then the dynamical behavior of the electronic servo-valve can be approximated by a first-order model [14] as

$$\frac{dX_v}{dt} + \frac{1}{\tau}X_v - \frac{K_v}{\tau}u = 0, \tag{14}$$

where τ is the time constant and K_v the gain of the servo-valve model.

From equations (7), (13), to (14), the dynamical equations of the actuator are summarized in equation (15). Here, the input signal is the current u and the output is the force F_{act}.

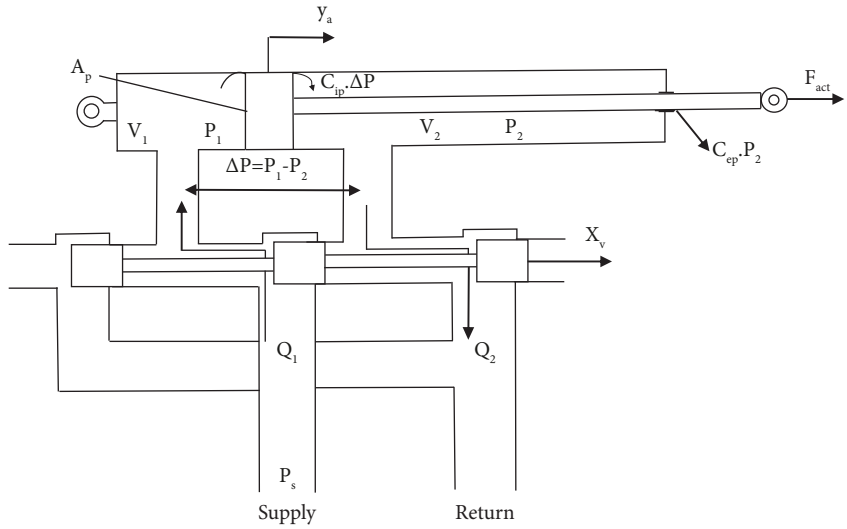

Figure 3: Diagram of the actuator for the active antiroll bar system [14, 17].

Table 2: Symbols of the actuator [14, 17].

Symbols	Description
A_P	Area of the piston
K_x	Valve flow gain coefficient
K_P	Total flow pressure coefficient
C_{tp}	Total leakage coefficient of the actuator
V_t	Total volume of trapped oil
β_e	Effective bulk modulus of the oil
τ	Time constant of the servo-valve
K_v	Servo-valve gain

$$\begin{cases} F_{\text{act}} = A_P \Delta P, \\ \dfrac{V_t}{4\beta_e}\dfrac{d\Delta P}{dt} + \left(K_P + C_{tp}\right)\Delta P - K_x X_v + A_P \dfrac{\mathrm{d}y_a}{\mathrm{d}t} = 0, \\ \dfrac{dX_v}{dt} + \dfrac{1}{\tau}X_v - \dfrac{K_v}{\tau}u = 0. \end{cases} \tag{15}$$

The torque generated by the active antiroll bar system at each axle is given by

$$U_i = l_{\text{act}} F_{\text{actri}} - l_{\text{act}} F_{\text{actli}}. \tag{16}$$

Here, l_{act} is half the distance between the two actuators, F_{acti} the actuator forces on the left and on the right.

The combination of equations (1)–(5) is the general equation to control the active antiroll bar system. The parameters of this system are found in [2, 4, 14].

3. H_∞ Control Synthesis of the Active Antiroll Bar System of Trucks

3.1. Background on H_∞ Control. The H_∞ control problem is formulated according to the generalized control structure shown in Figure 4 [4, 5, 23].

With P partitioned as

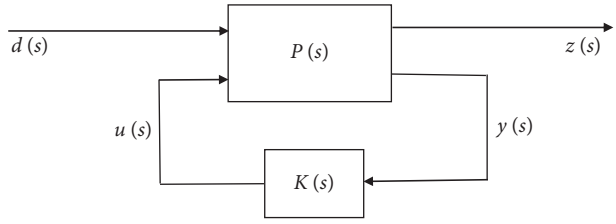

Figure 4: Generalized control structure.

$$\begin{bmatrix} z \\ y \end{bmatrix} = \begin{bmatrix} P_{11}(s) & P_{12}(s) \\ P_{21}(s) & P_{22}(s) \end{bmatrix} \begin{bmatrix} d \\ u \end{bmatrix}, \tag{17}$$

and $u = K(s).y$, which yields

$$\frac{z}{d} = F_l(P, K) \coloneqq = \left[P_{11} + P_{12}K\left[I - P_{22}K\right]^{-1}P_{21}\right]. \tag{18}$$

The aim is to design a controller K that stabilizes the closed-loop system and also reduces the signal transmission path from disturbances d to performance outputs z. This problem is then to find a controller K that minimizes γ such that

$$\left\|F_l(P, K)\right\|_\infty < \gamma. \tag{19}$$

By minimizing a suitably weighted version of $F_l(P, K)$ the control aim is achieved. The controller $y_K = K(s)u_K$ in any LTI system is represented as a state-space form as flows:

$$\begin{cases} \dot{x_K} = A_K x_K + B_K u_K, \\ y_K = C_K x_K + D_K u_K, \end{cases} \tag{20}$$

where, A_K, B_K, C_K, D_K are the matrices of the controller.

The interconnection of the controller and the open-loop system as $u_K = y(s)$, $y_K = u(s)$.

3.2. Control Objective and Problem Statement. The objective of the active antiroll bar control system is to maximize the

roll stability of the vehicle. Usually, an imminent rollover is detected when the calculated normalized load transfer ($R_{f,r}$) reaches 1 (or −1) [2]. The normalized load transfer $R = \pm 1$ corresponds to the most significant possible load transfer. In that case, the inner wheel in the bend lifts off.

While attempting to minimize the load transfer, it is also necessary to constrain the roll angles between the sprung and unsprung masses ($\phi - \phi_{tf,r}$) so that they stay within the limits of the suspension travel (7-8 deg) [2, 4, 5].

The performance characteristic that is most interesting when designing the active antiroll bar system is the normalized load transfer. The chosen control objective is to minimize the effect of the steering angle on the normalized load transfer $R_{f,r}$ in the H_∞ framework. As explained later, the limitation of the torques $U_{f,r}$ generated by the actuators is also crucial for practical implementation.

3.3. The First H_∞ Control Synthesis for the Active Antiroll Bar System. The closed-loop system is considered in Figure 5, which includes the feedback structure of the nominal model G, the controller K and the weighting functions W_{ij}. In this diagram, U_f and U_r are the control inputs, y_1 and y_2 are the measured outputs, n_1 and n_2 are the measurement noises. δ_f is the steering angle considered as a disturbance signal, which the driver sets. The variables e_1, e_2, e_3, e_4, and e_5 represent the performance outputs.

According to Figure 5, the concatenation of the linear model (6 and 15) with performance weighting functions leads to the state space representation of $P(s)$ [24]:

$$\begin{bmatrix} \dot{x}(t) \\ z(t) \\ y(t) \end{bmatrix} = \begin{bmatrix} A & B_1 & B_2 \\ C_1 & D_{11} & D_{12} \\ C_2 & D_{21} & D_{22} \end{bmatrix} \begin{bmatrix} x(t) \\ \mathrm{w}(t) \\ u(t) \end{bmatrix}, \tag{21}$$

with the disturbance input: $\mathrm{w}(t) = [d_1 \quad d_2\, d_3]^T$, the control input: $u(t) = [U_f\, U_r]^T$, the performance output: $z(t) = [e_1\, e_2\, e_3\, e_4\, e_5]^T$, the measured output: $y(t) = [a_y\, \phi]^T$. A, B_1, and B_2 are the matrices of the concatenation of the linear model. Meanwhile, C_1, D_{11}, and D_{12} are the matrices defined for the performance outputs of the control goals; C_2, D_{21}, and D_{22} are the determination matrices for the measured signals.

The weighting functions used in Figure 5 are the most important for designing the robust controller.

The input scaling weight W_{d1}, chosen as $W_{d1} = \pi/180$, normalizes the steering angle δ_f to the maximum expected value, corresponding to a 1^0 steering angle command.

The weighting functions W_{d2} and W_{d3} are selected as: $W_{d2} = W_{d3} = 0.01$, which accounts for small sensor noise models in the control design. The noise weights are chosen as 0.01 (m/s^2) for the lateral acceleration and 0.01(°/sec) for the derivative of the roll angle ϕ [2, 4]. Note that other low pass filters could be selected if needed.

The weighting functions W_{pi} represent the performance outputs (W_{p1}, W_{p2}, W_{p3}, W_{p4}, and W_{p5}). The purpose of the weighting functions is to keep small the control inputs, normalized load transfers, and the lateral acceleration over the desired frequency range. The weighting functions chosen for performance outputs can be considered as penalty functions. That is, weights should be prominent in the frequency range where small signals are desired and small where more significant performance outputs can be tolerated.

The weighting functions W_{p1} and W_{p2} corresponding to the front and rear control torques generated by active antiroll bars are chosen as

$$W_{p1} = \frac{1}{P_1}; \qquad W_{p2} = \frac{1}{P_2}. \tag{22}$$

The weighting functions W_{p3} and W_{p4} corresponding to the normalized load transfers at the front and rear axles are selected as

$$W_{p3} = \frac{1}{P_3}; \qquad W_{p4} = \frac{1}{P_4}. \tag{23}$$

The weighting function W_{p5} is selected as

$$W_{p5} = P_{51}\frac{P_{52}s + P_{53}}{P_{54}s + P_{55}}. \tag{24}$$

Here, the weighting function W_{p5} corresponds to a design that avoids the rollover with the driver's bandwidth in the frequency range of up to more than 4 rad/s [2, 23]. This weighting function will directly minimize the lateral acceleration when it reaches the critical value to avoid rollover.

The parameters P_{ij} are constant. From equations (22) to (24), the following variables P_1, P_2, P_3, P_4, P_{51}, P_{52}, P_{53}, P_{54}, and P_{55} are chosen as Table 3 [22, 23]. The selection of values of P_{ij} in the weight functions W_{pi} can be selected by the experience of the designer and must be paid through the process of testing, evaluation, and comparison to choose a reasonable value. In addition, it can also be combined with other optimization methods, such as genetic algorithms to determine their values [25–27].

Therefore, in the closed-loop system, the K_1 controller has the specified state-space matrices as follows:

(i) $A_{K1} = [2.672\ -1.402\ 0.2084\ -0.08157\ -3.922\ -6.447\ 5.901e-06;\ 93.1\ -6.57\ 1.157\ -0.5325\ -21.78\ -35.79\ 3.276e-05;\ 0.0002613\ -3.783e-06\ 1.73e-06\ 1\ -3.256e-05\ -5.352e-05\ 4.899e-11;\ 64.56\ -9.706\ 5.034\ -1.922\ -94.74\ -155.7\ 0.0001425;\ 9.579\ -0.8747\ 3.823\ 0.8872\ -26.02\ -2.79\ 8.114e-06;\ -3.006\ -0.2695\ 6.753\ 0.8712\ -0.1192\ -40.58\ 1.003e-05;\ -0.000241\ 3.489e-06\ -1.596e-06\ -2.535e-07\ 3.003e-05\ 4.936e-05\ -0.0001]$

(ii) $B_{K1} = [0.1724\ \ 0.01091;\ \ 2.032\ \ 0.205;\ \ 5.4e-06\ \ 2.585e-07;\ 2.587\ \ 0.1765;\ 0.266\ \ 0.01443;\ 0.01437\ \ 0.002626;\ 0.907\ \ 1.509e-06]$;

(iii) $C_{K1} = [1.032e+05\ \ -1.834e+04\ \ -3901\ \ -3899\ \ 6473\ \ 6908\ \ 0.3002\ \ 1.802e+05\ \ -3.287e+04\ \ -5764\ \ -6675\ \ 1.145e+04\ \ 1.211e+04\ \ 0.5256]$;

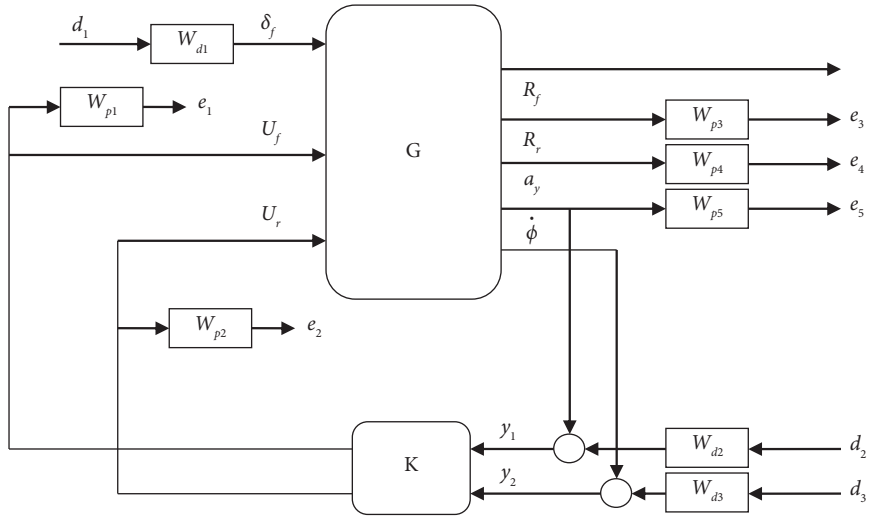

Figure 5: *G-K* control structure of the first H_∞ active antiroll bar control.

Table 3: The weighting functions of the H_∞ active antiroll bar controller.

W_{p1}	W_{p2}	W_{p3}	W_{p4}	W_{p5}				
P_1	P_2	P_3	P_4	P_{51}	P_{52}	P_{53}	P_{54}	P_{55}
150000	200000	0.760	1.050	1	0.0005	50	100	0.01

(iv) $D_{K1} = [6.18e-06\ 0;\ 1.099e-05\ 0]$.

3.4. The Second H_∞ Control Synthesis for the Active Antiroll Bar System. The design of the second H_∞ active antiroll bar controller is based on the first one, i.e., the control structure diagram is extended from Figure 5. The addition of two main contents includes two suspension roll angle sensors of the front and rear suspension systems, and these two signals are also considered as the performance outputs of the closed-loop control system.

Figure 6 shows the control structure diagram of the active antiroll bar system using the second H_∞ controller, where e_6, e_7 is the performance outputs for the two suspension roll angles. In order to reduce these two roll angles, two weighting functions W_{p6}, W_{p7} are used with values defined as $W_{p6} = W_{p7} = 1/0.5$.

Based on the first H_∞ controller and the control structure diagram in Figure 6, the state space representation of $P(s)$ has the disturbance input: $w(t) = [d_1 d_2 d_3 d_4 d_5]^T$, the control input: $u(t) = [U_f\ U_r]^T$, the performance output: $z(t) = [e_1\ e_2\ e_3\ e_4\ e_5\ e_6\ e_7]^T$, the measured output: $y(t) = [a_y\ \phi - \phi_{tf}\ \phi - \phi_{tr}\ \phi]^T$. Considering the performance outputs, including the suspension roll angle, make perfect sense. Because when studying the roll stability of automobiles in general and trucks in particular, the limit value of the suspension roll angle is from 7 to 8 degrees [2, 4, 5]. Therefore, in addition to reducing the normalized load transfer, it is also necessary to reduce the roll angle of the suspension system.

Therefore, in the closed-loop system, the K_2 controller has the specified state-space matrices as follows:

(i) $A_{K2} = [3.272\ -1.383\ -0.6932\ -0.2283\ -3.584\ -6.127\ 4.228e-06;\ 96.43\ -6.465\ -3.854\ -1.347\ -19.9\ -34.01\ 2.347e-05;\ 9.586e-11\ -1.305e-12\ -0.002227\ 1\ 0.001259\ 0.0009676\ 1.264e-17;\ 79.04\ -9.249\ -16.79\ -5.466\ -86.55–148\ 0.0001021;\ 10.39\ -0.8458\ 2.648\ 0.6878\ -25.68\ -2.282\ 5.873e-06;\ -1.977\ -0.2401\ 5.149\ 0.6195\ 0.5803–40.1\ 7.123e-06;–8.844e-11\ 1.204e-12\ -0.01636\ -1.93e-05\ 0.008129\ 0.008233\ -0.0001]$;

(ii) $B_{K2} = [7.505\ -0.1252\ -0.05453\ 0.4748;\ 88.47\ -0.5415\ -0.05149\ 8.923;\ 8.461e-11\ 0.09942\ 0.0764\ 9.562e-05;\ 112.6\ -0.6281\ -0.1142\ 7.683;\ 11.58\ -0.04497\ 0.002496\ 0.6282;\ 0.6254\ 0.02552\ 0.02093\ 0.1143;\ 39.48\ 0.6418\ 0.65\ 0.001524]$;

(iii) $C_{K2} = [3057\ -395.7–1061\ -258\ 390.4\ 617.8\ 0.005017;\ 5382\ -720\ -2067\ -456.7\ 1113\ 852.2\ 0.008576]$;

(iv) $D_{K2} = [6.18e-06\ 0\ 0\ 0;\ 1.099e-05\ 0\ 0\ 0]$.

4. Roll Stability Analysis in the Frequency Domain

In this section, the authors present the simulation results in the frequency domain with the forward velocity are considered at 70 km/h. The simulation result of the second H_∞ controller (continuous line) is compared with the first H_∞ controller (continuous-dotted line) and the passive antiroll bar system (dash line).

Figure 7 shows the transfer functions magnitude of the sprung mass roll angle ϕ due to the steering angle in the frequency domain. It can be seen that with two H_∞ controllers for the active antiroll bar system, the roll angle of the sprung mass decreases in the frequency range up to 9 rad/s. But with the second H_∞ controller for the active antiroll bar system, the roll angle of the sprung mass decreases more than the first one. Figures 8 and 9 show the transfer functions magnitude of the normalized load transfer at the front axle R_f and the rear axle R_r due to the steering angle in the frequency domain. It can be seen that with the two H_∞

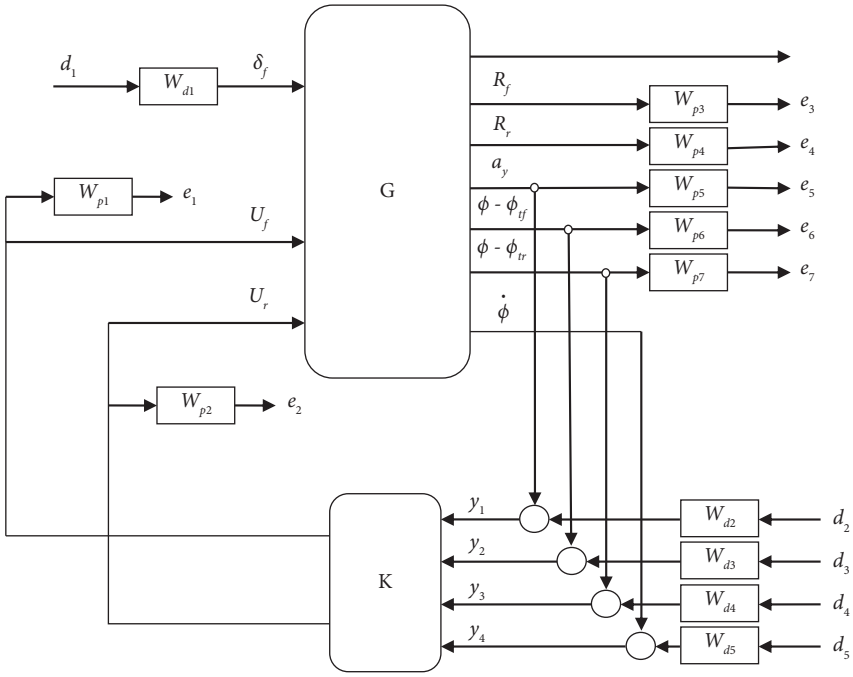

Figure 6: *G-K* control structure of the second H_∞ active antiroll bar control.

controllers for the active antiroll bar system, the normalized load transfers at the front axle decrease in the frequency range up to 7 rad/s.

Since the bandwidth of the steering angle when studying the roll stability of the vehicle reaches a maximum of 4 rad/s [2, 4], the corresponding comparison results from Figures 7–9 in the frequency domains at 10^{-5}, 10^{-4}, 1, and 4 rad/s are summarized in Table 4. In the last row, the authors make a comparison of the transfer functions magnitude of the considered signals at each frequency when comparing the case of using an active antiroll bar system with a second H_∞ controller and the subject of using a passive antiroll bar system. The comparison results show that the second H_∞ controller has significantly reduced the value of the transfer function magnitude from the steering angle. Thus, the consideration of using the suspension roll angle sensors has contributed substantially to reducing the value of the transfer function magnitude, thereby increasing the roll stability of the truck.

5. Roll Stability Analysis in the Time Domain

In this section, the authors evaluate the roll stability of the truck using the H_∞ active antiroll bar system in the time domain with three scenarios: (1) truck in a double lane change to avoid obstacle manoeuver; (2) truck in a double lane change to overtake manoeuver; and (3) truck in a cornering manoeuver.

5.1. Truck in a Double Lane Change to Avoid Obstacle Manoeuver. The truck manoeuver is a double lane change to avoid obstacles, which is often used to avoid an obstacle in an emergency. The manoeuver has a 2.5 m path deviation over 100 m. The size of the path deviation is chosen to test real obstacle avoidance in an emergency. The forward velocity is considered at 70 km/h. Figure 10 shows the steering angle, the roll angle of the sprung mass, the roll angle of the unsprung mass at the front axle and the roll angle of the unsprung mass at the rear axle. We can see that the first H_∞ active antiroll bar controller has significantly reduced (approximately 40%) the roll angles of the sprung mass, the unsprung mass at the front axle, and the roll angle of the unsprung mass at the rear axle compared to the passive antiroll bar system. And the second H_∞ active antiroll bar controller has decreased dramatically (approximately 55%), respectively.

Figure 11 shows the normalized load transfer and the roll angle of the suspension at the front and at the rear axle, respectively. We can see that the value of the normalized load transfer at the rear axle exceeds −1 at 2.8 seconds in the case of the passive antiroll bar system, but this value is within the limitation at the front axle. In two cases of H_∞ active antiroll bar controller, the roll stability is achieved because the limitation of the normalized load transfer is in the range from −1 to 1. The maximum of absolute values of the roll angle of the suspensions is always less than 7-8 (deg), so they are within the limitations of the suspension travel. When compared with the passive system, we can see that the first H_∞ active antiroll bar controller has significantly reduced (approximately 40%) and the second H_∞ active antiroll bar controller has decreased substantially (about 55%) the normalized load transfer and the roll angle of suspension at the front and the rear axles, respectively.

The simulation results when the truck in a double lane change to avoid obstacle manoeuver clearly shows the effectiveness of the second H_∞ active antiroll bar controller in using the sensors of the suspension roll angle.

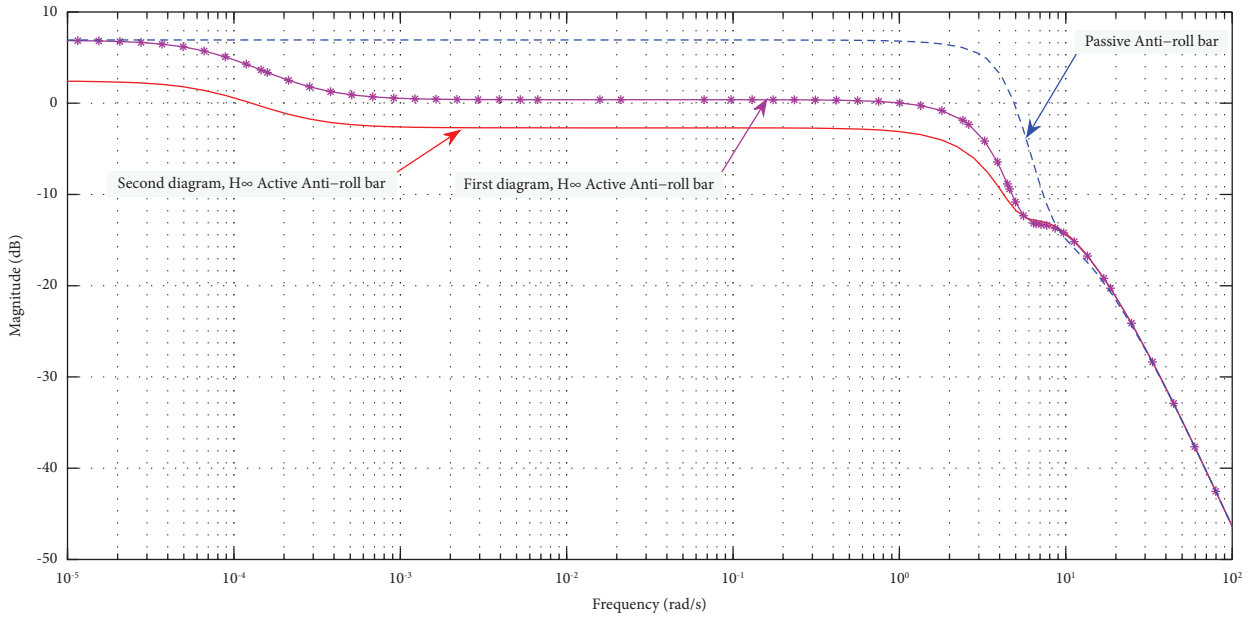

Figure 7: Transfer function magnitude of the sprung mass roll angle (ϕ) due to the steering angle.

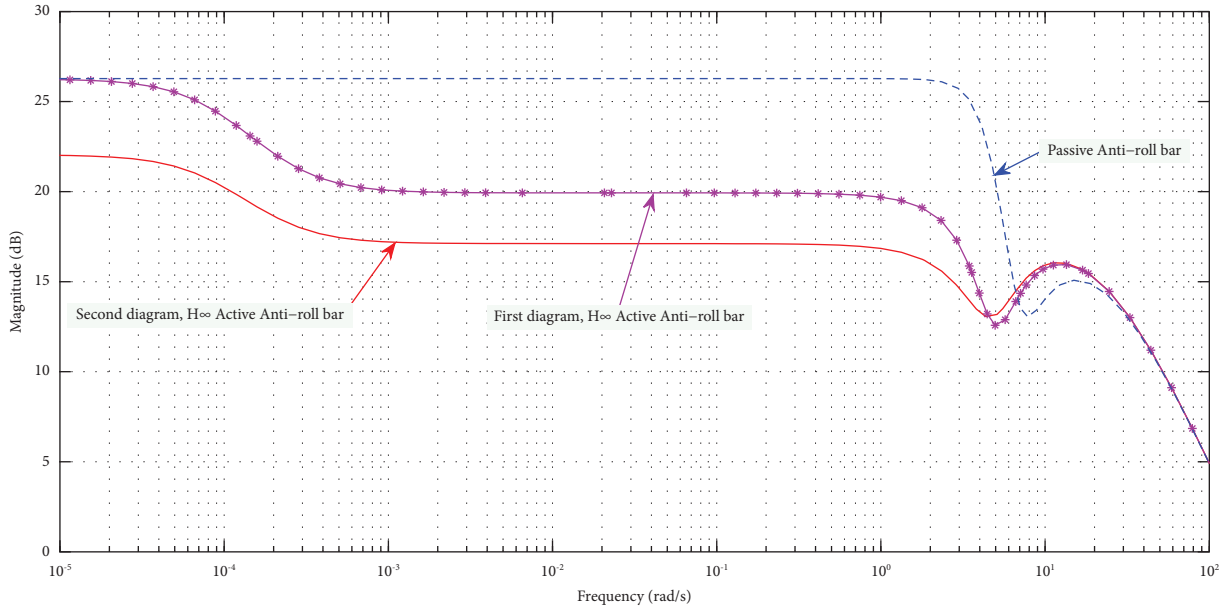

Figure 8: Transfer function magnitude of the normalized load transfer at the front axle (R_f) due to the steering angle.

5.2. Truck in a Double Lane Change to Overtake Manoeuver. In this subsection, the authors introduce the time responses of a truck in a double lane change to overtake a manoeuver. Figure 12 shows the steering angle, the roll angle of the sprung mass, and the roll angles of the unsprung mass at the front and rear axles. When compared with the passive antiroll bar system, we can see that the first H_∞ active antiroll bar controller has significantly reduced (approximately 41%) and the second H_∞ active antiroll bar controller has diminished considerably (about 53%) for the roll angle of the sprung mass, the roll angle of the unsprung mass at the front and rear axles.

Figure 13 shows the normalized load transfer and the suspension roll angle at the front and rear axles. We can see that the values of normalized load transfer are always in the range from −1 to 1 and the maximum absolute values of the roll angle of the suspensions are always less than 7-8 (deg). When we compare it with the passive system, we can see that the first H_∞ active antiroll bar controller has significantly reduced (approximately 38%) and the second H_∞ active antiroll bar controller has significantly reduced (approximately 54%) the normalized load transfer and the roll angle of suspension at the front and rear axles, respectively.

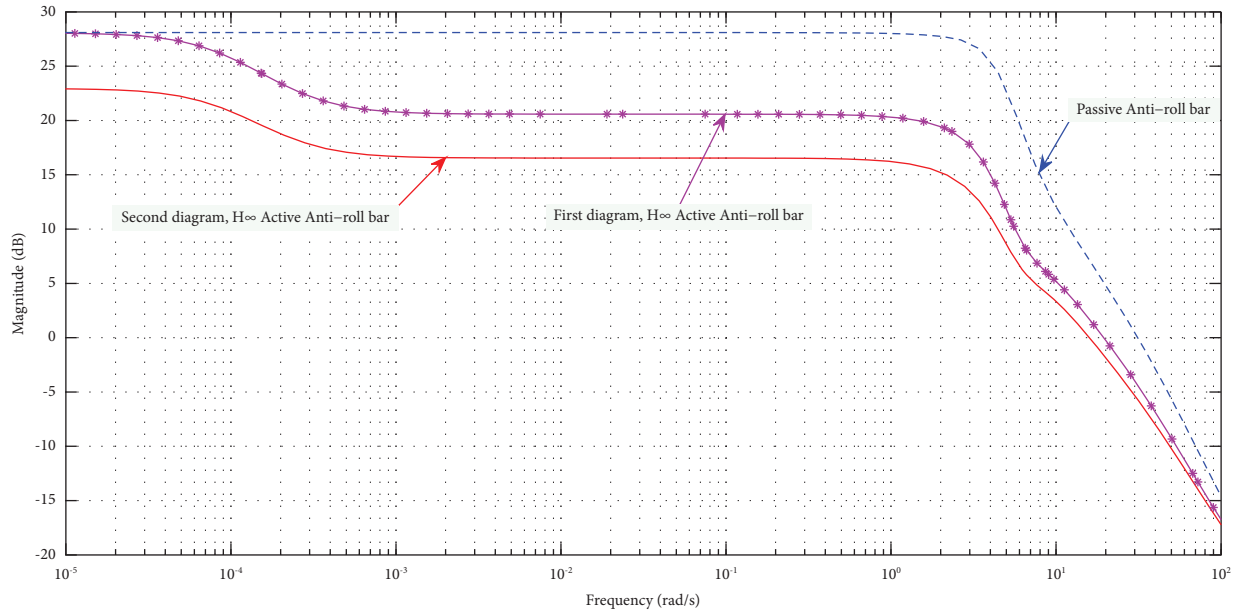

Figure 9: Transfer function magnitude of the normalized load transfer at the rear axle (R_r) due to the steering angle.

Table 4: Comparison results in the frequency domain.

	10^{-5} (rad/s)			10^{-4} (rad/s)			1 (rad/s)			4 (rad/s)		
	ϕ (dB)	R_f (dB)	R_r (dB)	ϕ (dB)	R_f (dB)	R_r (dB)	ϕ (dB)	R_f (dB)	R_r (dB)	ϕ (dB)	R_f (dB)	R_r (dB)
Passive	7.5	27	27.5	7.5	27	27.5	7.5	27	27.5	0	24	25
First H_∞	7.5	27	27.5	5	24	26	0.5	20	20	−11	14	15
Second H_∞	3	22	23	1	20	21	−4	17	17	−12	13	8
Reduction (compared with passive)	4.5	5	4.5	6.5	7	6.5	11.5	10	10.5	12	11	17

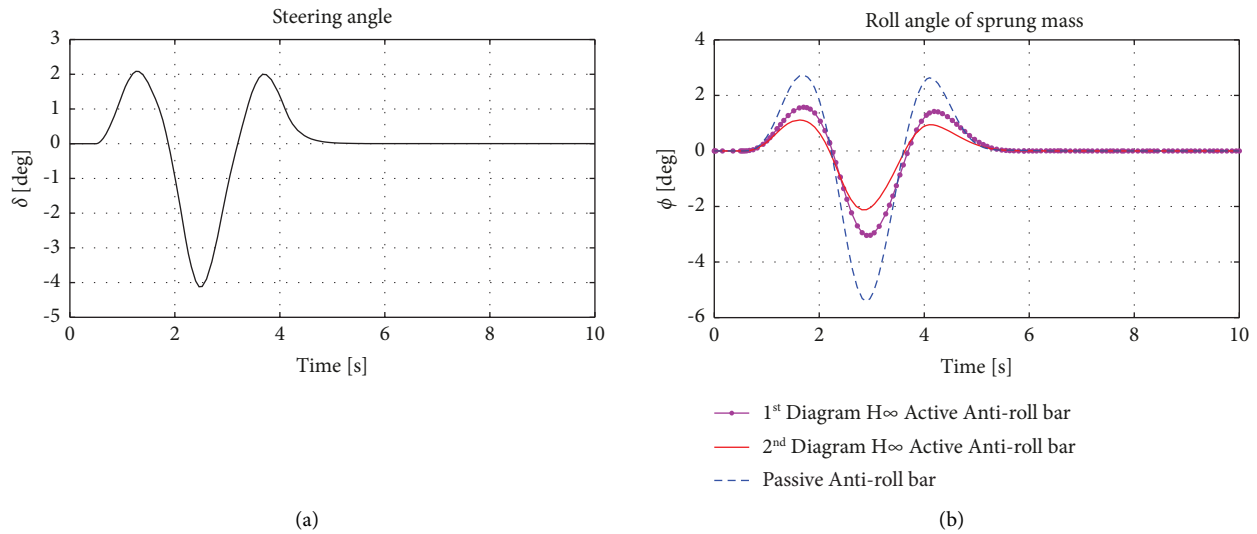

(a) (b)

Figure 10: Continued.

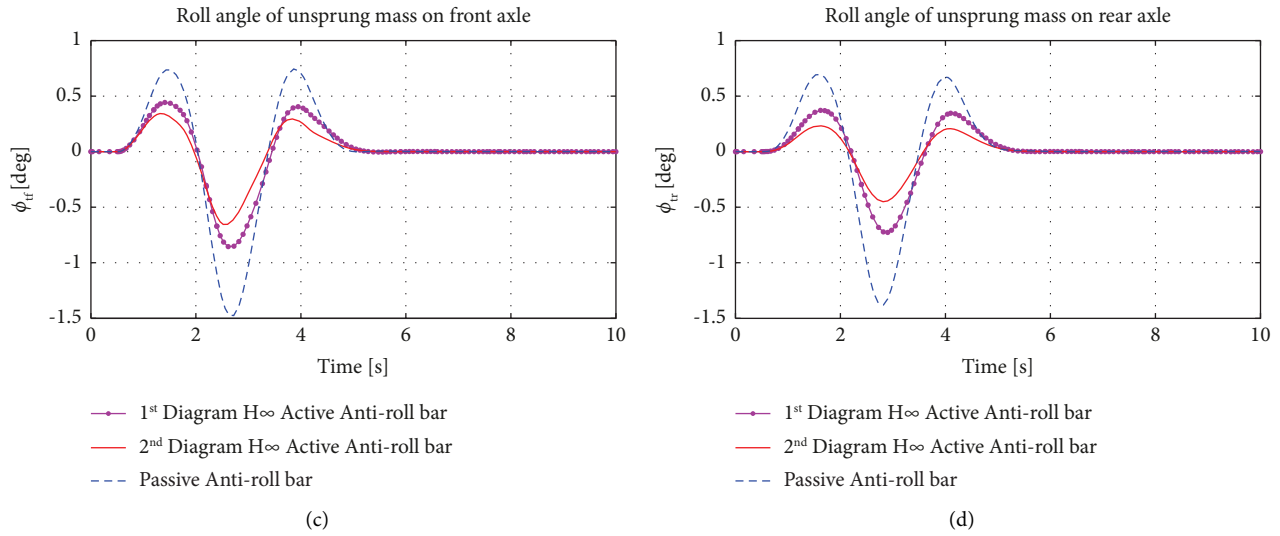

Figure 10: Time responses of the steering angle, roll angle of the sprung mass, and unsprung masses of the truck: in a double lane change to avoid obstacle manoeuver. (a) Steering angle. (b) Roll angle of sprung mass. (c) Roll angle of unsprung mass of the front axle. (d) Roll angle of unsprung mass of the rear axle.

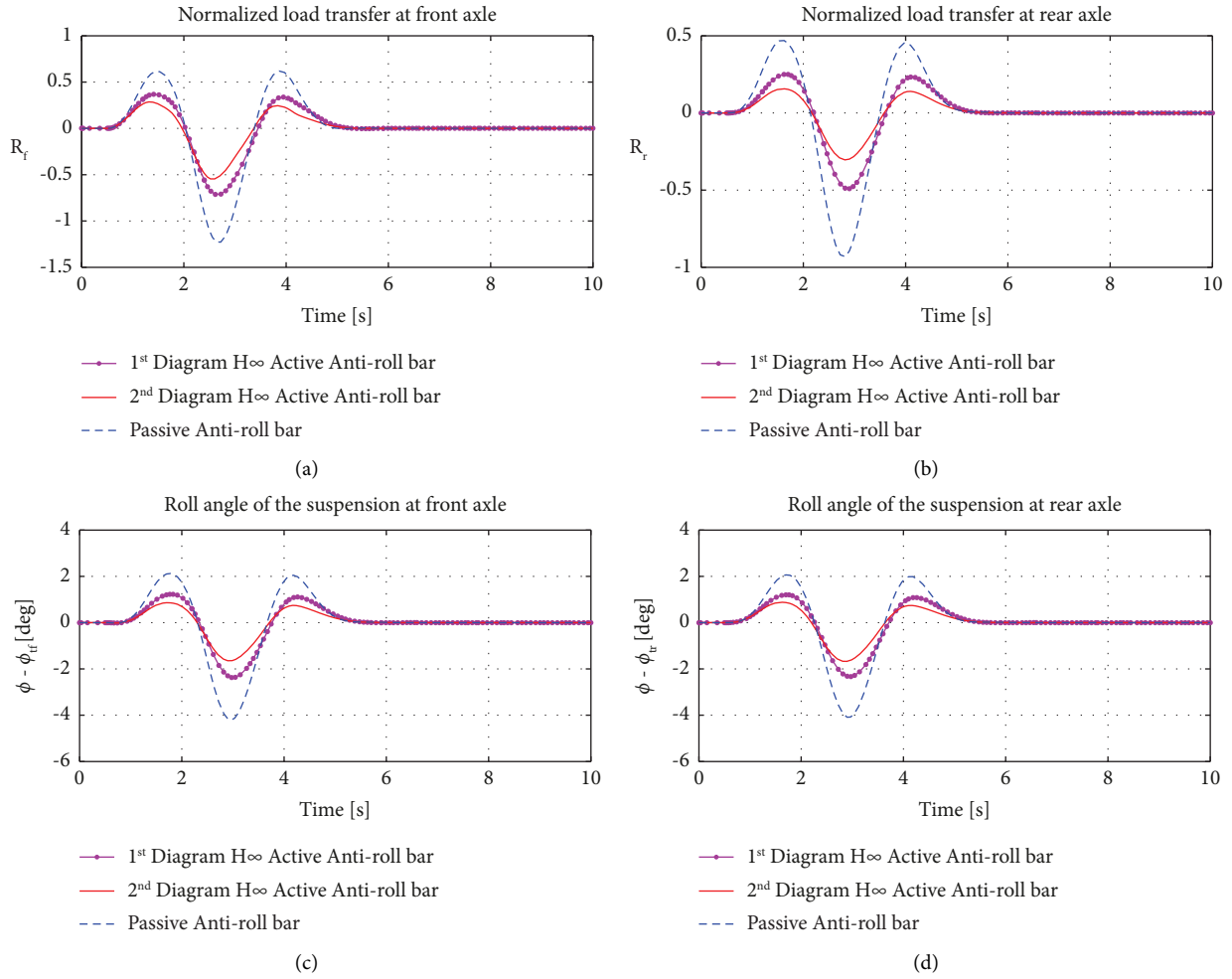

Figure 11: Time responses of normalized load transfer and roll angle of suspension on two axles of the truck: in a double lane change to avoid obstacle manoeuver. (a) Normalized load transfer at the front axle. (b) Normalized load transfer at the rear axle. (c) Roll angle of the suspension at the front axle. (d) Roll angle of the suspension at the rear axle.

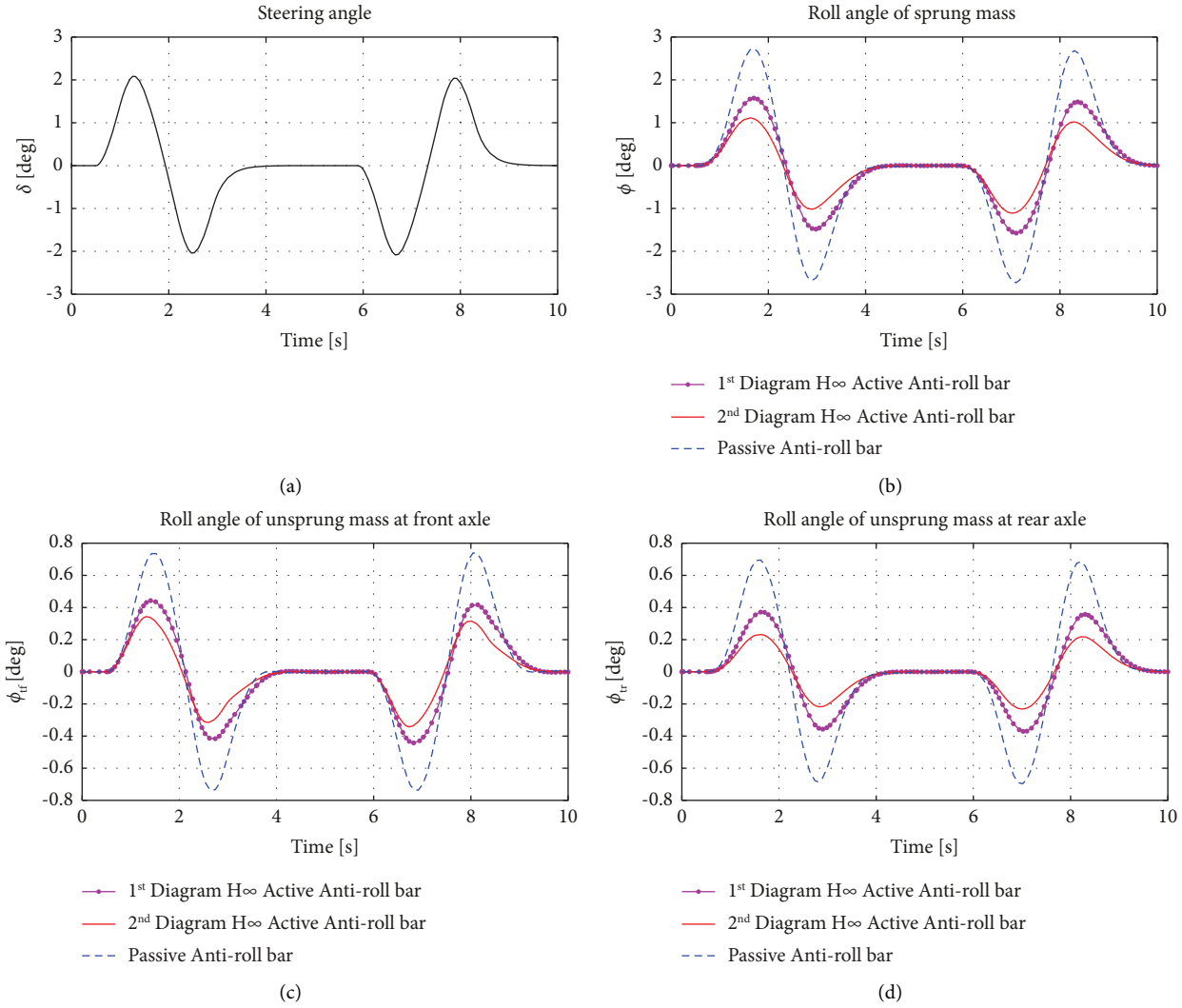

Figure 12: Time responses of the steering angle and roll angle of the sprung mass and unsprung masses of the truck: in a double lane change to overtake manoeuver. (a) Steering angle. (b) Roll angle of sprung mass. (c) Roll angle of unsprung mass at the front axle. (d) Roll angle of unsprung mass at the rear axle.

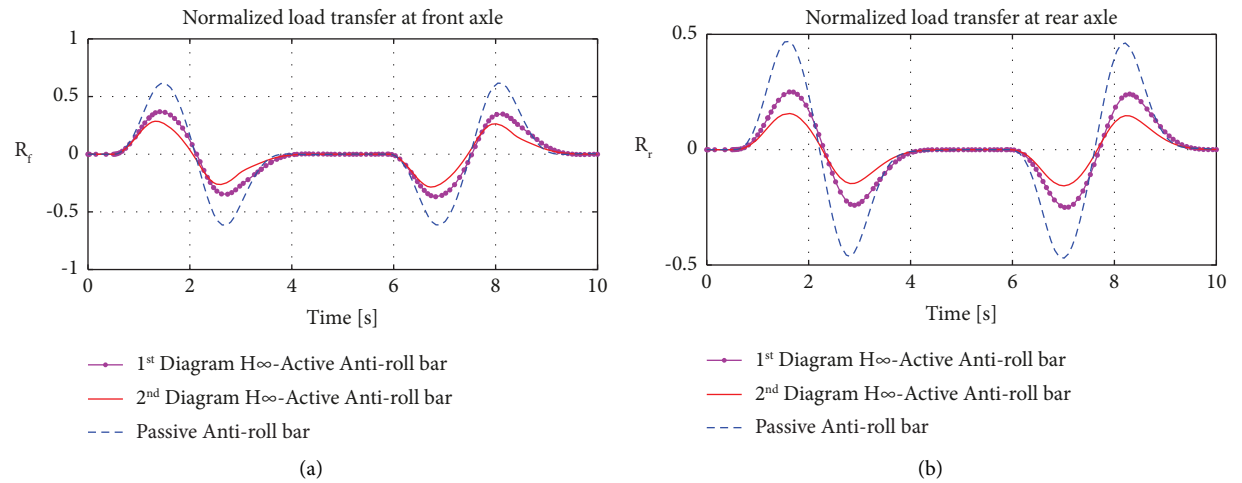

Figure 13: Continued.

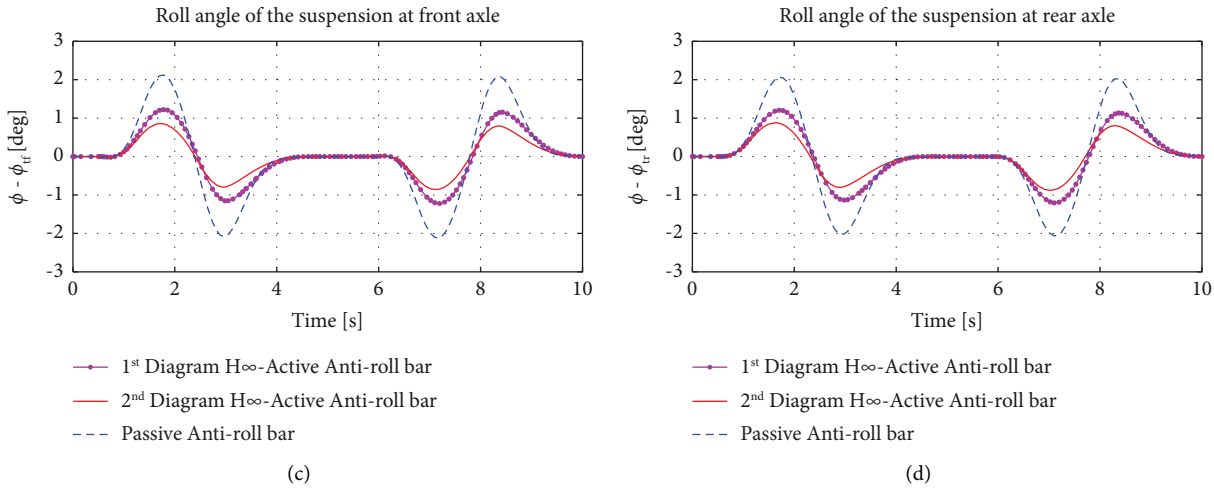

FIGURE 13: Time responses of normalized load transfer and roll angle of suspension on the axles of the truck: in a double lane change to overtake manoeuver. (a) Normalized load transfer at the front axle. (b) Normalized load transfer at the rear axle. (c) Roll angle of the suspension at the front axle. (d) Roll angle of the suspension at the rear axle.

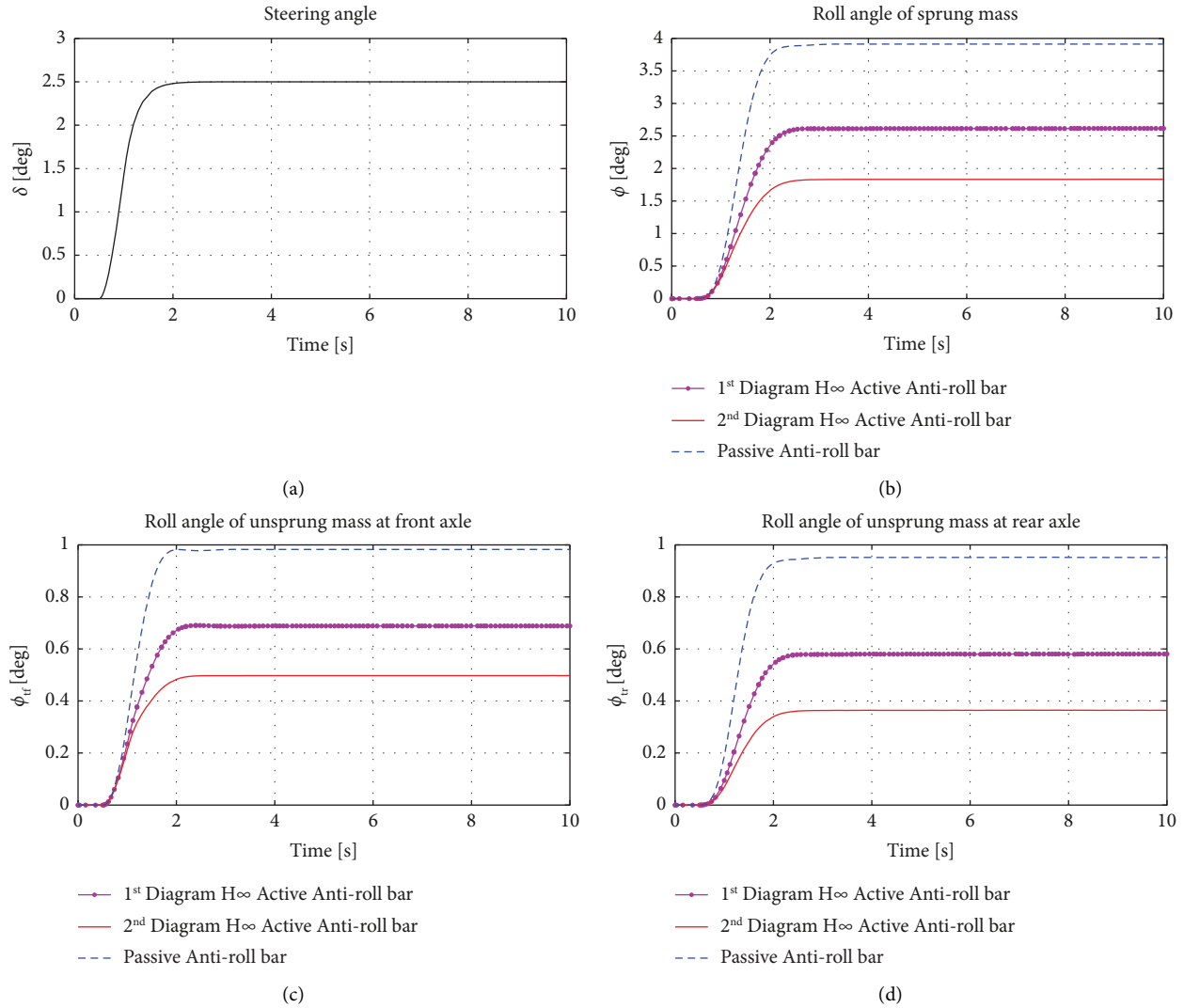

FIGURE 14: Time responses of the steering angle and roll angle of the sprung mass and unsprung masses of the truck: in a cornering manoeuver. (a) Steering angle. (b) Roll angle of sprung mass. (c) Roll angle of unsprung mass at the front axle (d) Roll angle of unsprung mass at the rear axle.

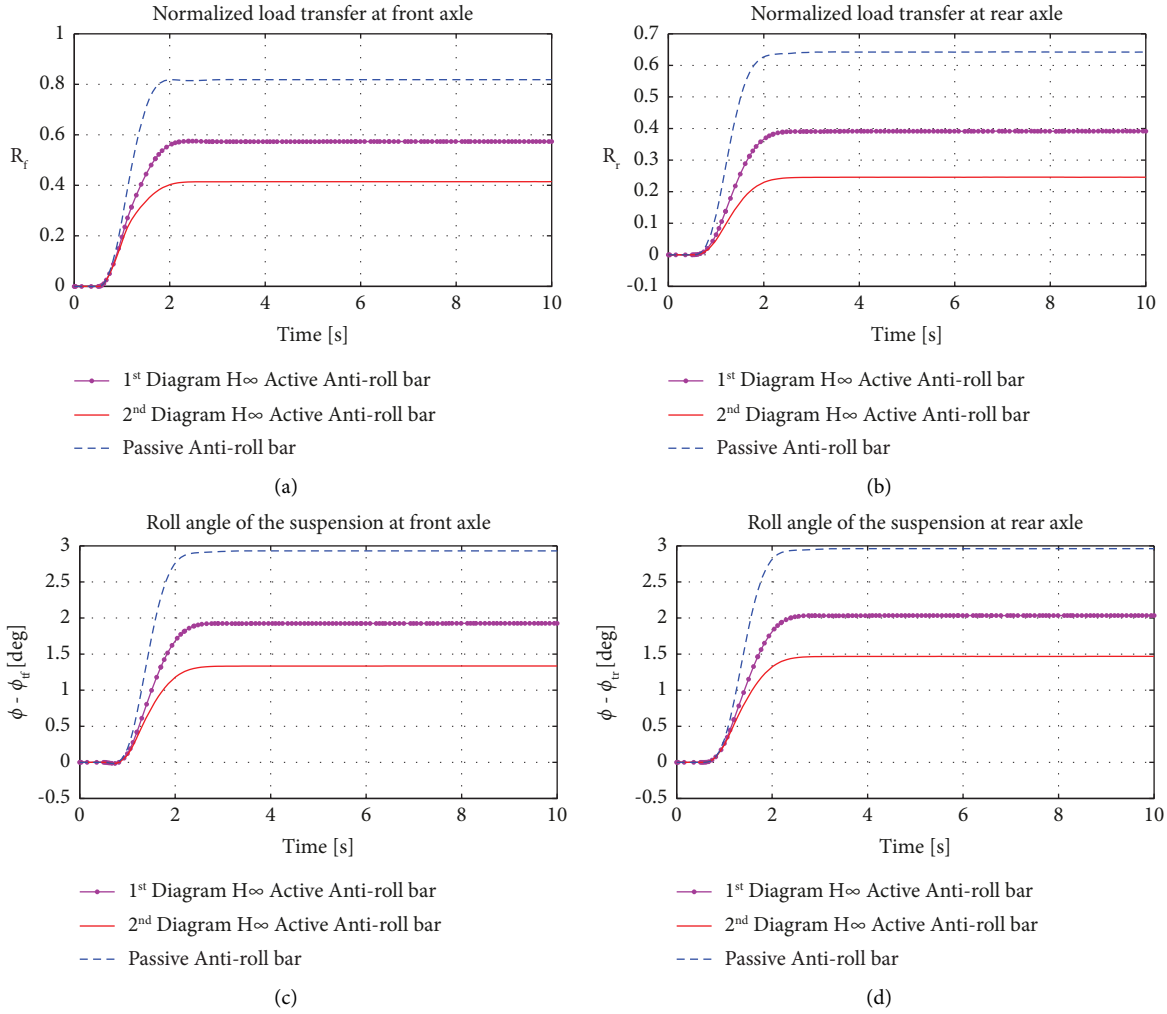

Figure 15: Time responses of normalized load transfer and roll angle of suspension on the axles of the truck: in a cornering manoeuver. (a) Normalized load transfer at the front axle. (b) Normalized load transfer at the rear axle. (c) Roll angle of the suspension at the front axle. (d) Roll angle of the suspension at the rear axle.

5.3. Truck in a Cornering Maneuver. The final scenario used to evaluate the performance of the proposed $H\infty$ controller is when the truck is in a cornering maneuver, which is a very common case of the rollover phenomenon. In this case, the lateral acceleration is inversely proportional to the radius of the trajectory, and the truck has a high center of gravity and a heavy load, the possibility of a rollover accident also increases. Figure 14 shows the steering angle, the roll angle of the sprung mass, and the roll angles of the unsprung masses at the front and rear axles. When the steering angle increases, i.e., the truck turns around, the values of the angles also increase and reach a stable value when the driver keeps the steering wheel at 2.5 (deg). From 2.5 s, the roll angle of the sprung mass reaches 3.8 (deg) with the passive antiroll bar system, while with the first H_∞ active antiroll bar controller, this value reaches 2.6 (deg), and with the second H_∞ active antiroll bar controller, this value reaches 1.8 (deg). Thus, compared to the first H_∞ active antiroll bar controller, the roll angle of the sprung mass using the second H_∞ active antiroll bar controller has been reduced by about 20%.

Figure 15 shows the results of the evaluation of the normalized load transfer at the two axles and the roll angles of the suspension system. The response according to the steering angle of the above signals is very suitable. When the truck used the second H_∞ active antiroll bar controller, the normalized load transfer is reduced by 50% compared with the passive antiroll bar system and about 20% compared with the first H_∞ active antiroll bar controller. Similar results are evident in the roll angle of the suspension system at the two axles.

Simulation results in the time domain with different scenarios reinforce the results in the frequency domain. Therefore, it can be asserted that the use of the suspension roll angle sensors has improved the efficiency of the active antiroll bar system using the robust control method.

6. Conclusions

This article has focused on studying the influence of the suspension roll angle sensors on the efficiency of the active antiroll bar system using robust controllers. A truck model

was first introduced to solve that goal, and the dynamics equation was written as a state space representation. Then, a basic structure of an active antiroll bar system with the robust control method (first H_∞ active antiroll bar controller) was described in detail. Then, a full controller for the active antiroll bar system (second H_∞ active antiroll bar controller) is proposed considering the information from the suspension roll angle sensors, and this is also the performance output considered. Simulation results in the frequency domain and time domain with different scenarios have clearly shown that the effectiveness of the active antiroll bar system using the suspension roll angle sensors has improved the efficiency compared to the basic controller by about 20% and about 50% when compared with the passive antiroll bar system.

Further research can be conducted to examine the effect of measurement noise on the performance of an active antiroll bar system.

Appendix

A: The matrices of equation (6)

The state space representation of the system is

$$\begin{cases} \dot{x} = Ax + B_1 w + B_2 u, \\ y = Cx. \end{cases} \tag{A.1}$$

The state vector: $x = [\beta\ \dot{\psi}\ \varphi\ \dot{\varphi}\ \varphi_{uf}\ \varphi_{ur}]^T$, the disturbance input: $w = [\delta_f]$, the control inputs: $u = [U_f\ U_r]^T$, and the output vector: $y = [\beta\ \dot{\psi}\ \varphi\ \dot{\varphi}\ \varphi_{uf}\ \varphi_{ur}]^T$. The matrices A, B_1, and B_2 are defined as: $A = E^{-1}.A_0; B_1 = E^{-1}.B_{01}; B_2 = E^{-1}.B_{02}$.

With

$$E = \begin{bmatrix} m.v & 0 & 0 & -m_s.h & 0 & 0 \\ 0 & I_{zz} & 0 & -I_{xz} & 0 & 0 \\ -m_s.v.h & -I_{xz} & 0 & I_{xx} + m_s.h^2 & -b_f & -b_r \\ -m_{uf}.v.\left(r - h_{uf}\right) & 0 & 0 & 0 & b_f & 0 \\ -m_{ur}.v.\left(r - h_{ur}\right) & 0 & 0 & 0 & 0 & b_r \\ 0 & 0 & 1 & 0 & 0 & 0 \end{bmatrix},$$

$$A_0 = [\ A_{01}\ \ A_{02}\ ]$$

$$A_{01} = \begin{bmatrix} -\mu\left(C_f + C_r\right) & \mu.\dfrac{C_r.l_r - C_f.l_f}{v} - m.v & 0 \\ \mu.\left(C_r.l_r - C_f.l_f\right) & -\mu.\dfrac{C_r.l_r^2 - C_f.l_f^2}{v} & 0 \\ 0 & m_s.v.h & m_s.g.h - k_f - k_r \\ -\mu.C_f.r & m_{uf}.v.\left(r - h_{uf}\right) - \mu.\dfrac{C_f.l_f.r}{v} & k_f \\ -\mu.C_r.r & m_{ur}.v.\left(r - h_{ur}\right) + \mu.\dfrac{C_f.l_f.r}{v} & k_r \\ 0 & 0 & 0 \end{bmatrix},$$

$$A_{02} = \begin{bmatrix} 0 & 0 & 0 \\ 0 & 0 & 0 \\ -\left(b_f + b_r\right) & k_f & k_r \\ b_f & m_{uf}.g.h_{uf} - k_f - k_{tf} & 0 \\ b_r & 0 & -\left(m_{ur}.g.h_{ur} - k_r - k_{tf}\right) \\ 1 & 0 & 0 \end{bmatrix},$$

$$B_{01} = \begin{bmatrix} \mu.C_f \\ \mu.C_f.l_f \\ 0 \\ \mu.C_f.r \\ 0 \\ 0 \end{bmatrix}; \tag{A.2}$$

$$B_{02} = \begin{bmatrix} 0 & 0 \\ 0 & 0 \\ 1 & 1 \\ 1 & 0 \\ 0 & 1 \\ 0 & 0 \end{bmatrix}.$$

Some notations are used as follows: $Y_{\beta f} = -\mu.C_f$, $Y_{\dot{\psi} f} = -\mu.l_f.C_f/v$, $Y_{\beta r} = -\mu.C_r$, $Y_{\dot{\psi} r} = -\mu.l_r.C_r/v$, $Y_\beta = Y_{\beta r} + Y_{\beta r} = -\mu.(C_f + C_r)$, $Y_{\dot{\psi}} = Y_{\dot{\psi} f} + Y_{\dot{\psi} r} = -\mu.(l_r.C_r - l_f.C_f/v)$, $Y_\delta = \mu.C_f$, $N_\beta = \mu.(l_r.C_r - l_f.C_f)$, $N_{\dot{\psi}} = \mu.(l_r^2.C_r + l_f^2.C_f/v)$, $N_{\dot{\psi}} = \mu.l_f.C_f$,

The matrices A_0, B_{01} are re-written as

$$A_0 = \begin{bmatrix} Y_\beta & Y_{\dot{\psi}} - m.s & 0 & 0 & 0 & 0 \\ N_\beta & N_{\dot{\psi}} & 0 & 0 & 0 & 0 \\ 0 & m_s.v.h & m_s.g.h - k_f - k_r & -\left(b_f + b_r\right) & k_f & k_r \\ r.Y_{\beta f} & m_{uf}.v.\left(r - h_{uf}\right) + r.Y_{\dot{\psi} f} & k_f & k_r & m_{uf}.g.h_{uf} - k_f - k_r & 0 \\ r.Y_{\beta r} & m_{ur}.v.(r - h_{ur}) + r.Y_{\dot{\psi} r} & k_r & b_r & 0 & -(m_{ur}.g.h_{ur} + k_r + k_{tr}) \\ 0 & 0 & 0 & 1 & 0 & 0 \end{bmatrix},$$

$$B_{01} = \begin{bmatrix} Y_\delta \\ N_\delta \\ 0 \\ r.Y_\delta \\ 0 \\ 0 \end{bmatrix}. \tag{A.3}$$

The matrix C is

$$C = \begin{bmatrix} 1 & 0 & 0 & 0 & 0 & 0 \\ 0 & 1 & 0 & 0 & 0 & 0 \\ 0 & 0 & 1 & 0 & 0 & 0 \\ 0 & 0 & 0 & 1 & 0 & 0 \\ 0 & 0 & 0 & 0 & 1 & 0 \\ 0 & 0 & 0 & 0 & 0 & 1 \end{bmatrix}. \quad (A.4)$$

Data Availability

The steering angle data used to support the findings of this study are included within the article.

Conflicts of Interest

The authors declare that they have no conflicts of interest.

References

[1] M. Boada, B. Boada, A. Quesada, A. Gaucha, and V. Daz, "Active roll control using reinforcement learning for a single unit heavy vehicle," in *Proceedings of the 12th IFToMM World Congress*, Besancon, France, July 2007.

[2] P. Evgenikos, G. Yannis, K. Folla, R. Bauer, K. Machata, and C. Brandstaetter, "Characteristics and causes of heavy goods vehicles and buses accidents in europe," *Transportation Research Procedia*, vol. 14, pp. 2158–2167, 2016.

[3] G. Morrison and D. Cebon, "Combined emergency braking and turning of articulated heavy vehicles," *Vehicle System Dynamics*, vol. 55, no. 5, pp. 725–749, 2017.

[4] P. Gaspar, I. Szaszi, and J. Bokor, "The design of a combined control structure to prevent the rollover of heavy vehicles," *European Journal of Control*, vol. 10, no. 2, pp. 148–162, 2004.

[5] P. Gaspar, I. Szaszi, and J. Bokor, "Reconfigurable control structure to prevent the rollover of heavy vehicles," *Control Engineering Practice*, vol. 13, no. 6, pp. 699–711, 2005.

[6] P. Gaspar, Z. Szabo, and J. Bokor, "Prediction based combined control to prevent the rollover of heavy vehicles," in *Proceedings of the 13th Mediterranean Conference on Control and Automation*, Limassol, Cyprus, July 2005.

[7] H. Imine, L. M. Fridman, and T. Madani, "Steering control for rollover avoidance of heavy vehicles," *IEEE Transactions on Vehicular Technology*, vol. 61, no. 8, pp. 3499–3509, 2012.

[8] J. He, D. A. Crolla, M. C. Levesley, and W. J. Manning, "Coordination of active steering, driveline, and braking for integrated vehicle dynamics control," *Proceedings of the Institution of Mechanical Engineers - Part D: Journal of Automobile Engineering*, vol. 220, no. 10, pp. 1401–1420, 2006.

[9] X. Li, J. Li, L. Su, and Y. Cao, "Control methods for roll instability of articulated steering vehicles," *Mathematical Problems in Engineering*, vol. 2016, Article ID 8041816, 14 pages, 2016.

[10] A. L. Do, B. Soualmi, J. Lozoya-Santos, O. Sename, L. Dugard, and R. Ramirez-Mendoza, "Optimization of weighting function selection for H∞ control of semi-active suspensions," in *Proceedings of the 12th Mini Conference on Vehicle System Dynamics, Identification and Anomalies (VSDIA 2010)*, Budapest, Hungary, July 2010.

[11] A. J. P. Miège, *Development of active anti-roll control for heavy vehicles*, PhD thesis, University of Cambridge, London, UK, 2000.

[12] L. Palkovics, S. Semsey, and E. Gerum, "Roll-over prevention system for commercial vehicles - additional sensorless function of the electronic brake system," *Vehicle System Dynamics*, vol. 32, no. 4-5, pp. 285–297, 1999.

[13] D. J. Sampson and D. Cebon, "Active roll control of single unit heavy road vehicles," *Vehicle System Dynamics*, vol. 40, no. 4, pp. 229–270, 2003.

[14] Vu Van Tan, *Enhancing the roll stability of heavy vehicles by using an active anti-roll bar system*, University Grenoble, Alpes, France, Phd Thessis, 2017.

[15] D. Sampson and D. Cebon, "An investigation of roll control system design for articulated heavy vehicles," in *Proceedings of the 4th International symposium on Advanced Vehicle Control, AVEC1998*, Nagoya, Japan, June 1998.

[16] D. J. M. Sampson and D. Cebon, "Achievable roll stability of heavy road vehicles," *Proceedings of the Institution of Mechanical Engineers - Part D: Journal of Automobile Engineering*, vol. 217, no. 4, pp. 269–287, United Kingdom, 2003.

[17] V. T. Vu, O. Sename, L. Dugard, and P. Gaspar, "Active anti-roll bar control using electronic servo-valve hydraulic damper on single unit heavy vehicle," in *Proceedings of the IFAC Symposium on Advances in Automotive Control - 8th AAC 2016*, Sweden, Europe, July 2016.

[18] Z. Yu, "Anti-rollover control algorithm for heavy semi-trailer based on LQG," in *Proceedings of the 2010 IEEE International Conference on Information and Automation*, Harbin, China, July 2010.

[19] D. E. Goldberg and K. Sastry, *Genetic Algorithms: The Design of Innovation*, Springer, New York, NY, 2020.

[20] X.-S. Li, Y.-Y. Ren, and X.-L. Zheng, "Model-free adaptive control for tank truck rollover stabilization," *Mathematical Problems in Engineering*, vol. 2021, Article ID 8417071, 16 pages, 2021.

[21] M. A. Rodríguez Licea, E. A. Vazquez Rodriguez, F. J. Perez Pinal, and J. Prado Olivares, "The rollover risk in delta tricycles: a new rollover index and its robust mitigation by rear differential braking," *Mathematical Problems in Engineering*, vol. 2018, Article ID 4972419, 14 pages, 2018.

[22] V. T. Vu, O. Sename, L. Dugard, and P. Gaspar, "H∞ active anti-roll bar control to prevent rollover of heavy vehicles: a robustness analysis," in *Proceedings of the IFAC Symposium on System Structure and Control - 6th SSSC 2016*, Turkey, December 2016, https://www.google.com/search?q=Ankara&stick=H4sIAAAAAAAAAONgVmLXz9U3yKosf8RoxC3w8sc9YSnNSWtOXmNU5uIKzsgvd80rySypFBLlYoOyuKU4uWB6eBaxsjnmZScWJQIA0XQQMUkAAAA&sa=X&ved=2ahUKEwjshu-9ka78AhV-R2wGHRw0BJgQzIcDKAB6BAgOEAE.

[23] V. T. Vu, O. Sename, L. Dugard, and P. Gaspar, "Optimal selection of weighting functions by genetic algorithms to design H∞ Anti-roll bar controllers for heavy vehicles," in *Proceedings of the VSDIA 2016 - 15th Mini Conference on Vehicle System Dynamics, Identification and Anomalies*, Budapest. Hungary, November 2016, https://hal.archives-ouvertes.fr/hal-01361861/document.

[24] V. V. Tan, O. Sename, and P. Gaspar, "Improving roll stability of tractor semi-trailer vehicles by using H∞ active anti-roll bar control system," *Proceedings of the Institution of Mechanical Engineers - Part D: Journal of Automobile Engineering*, vol. 235, no. 14, pp. 3509–3520, 2021.

[25] A. Sahinkaya, T. Jerzy, and Sawicki, "Application of genetic algorithm for synthesis of H∞ controllers for active magnetic bearing systems," in *Proceedings of the 10th International Conference on Rotor Dynamics - IFToMM*, switzerland, Europe, January 2019.

[26] I. Kitsios and T. Pimenides, "Hoo controller design for a distillation column using genetic algorithms," *Mathematics and Computers in Simulation*, vol. 60, no. 3-5, pp. 357–367, 2002.

[27] M. Zhang, L. Gou, Z. Jiang, and C. Sun, "Optimization of aero-engine H-infinity robust controller based on quantum genetic algorithm," in *Proceedings of the 2021 12th International Conference on Mechanical and Aerospace Engineering (ICMAE)*, pp. 225–231, Athens, Greece, July 2021.